applied sciences

MDPI

Article

Enhanced Photocatalytic Performance of $Bi_2O_2CO_3$ Loaded Activated Carbon for Toluene Removal in Air

Xiaoyan Wang [1], Lu Chen [1], Changfu Li [1], Yongchao Xiao [1], Yuchen Gao [1], Yaochun Liu [2], Yuanhua Lin [3,*] and Junping Ding [1,*]

1 China Astronaut Research and Training Center, Beijing 100094, China
2 Foshan (Southern China) Institute for New Materials, Foshan 528200, China
3 State Key Laboratory of New Ceramics and Fine Processing, School of Materials Science and Engineering, Tsinghua University, Beijing 100084, China
* Correspondence: linyh@mail.tsinghua.edu.cn (Y.L.); djp15@tsinghua.org.cn (J.D.); Tel.: +86-10-6636-5775 (J.D.)

Featured Application: This work may provide potential applications in indoor air purification for the removal of volatile organic compounds.

Abstract: Activated carbon (AC) is one of the most used air purification materials with excellent adsorption capacity for volatile organic compounds (VOCs). In this work, $Bi_2O_2CO_3$ (BOC) nanomaterials, as a photocatalysis component, are grown on the surface of the AC to construct BOC/AC composites. The as-synthesized composites were characterized by scanning electron microscopy (SEM), X-ray diffraction (XRD), and N_2 adsorption/desorption measurements. The results demonstrate that flower-like BOC can be grown in situ on the surface of AC. The photocatalytic properties for the removal of gaseous toluene (50.0 ppm) in air over the BOC/AC composites were investigated under simulated sunlight illumination. The results show that the BOC/AC photocatalyst can effectively degrade toluene to CO_2 and H_2O, with more than 90% degradation in 3 h. The excellent photocatalytic performance of the BOC/AC composite catalyst can be ascribed to the synergistic effect of the adsorption ability of AC and photocatalytic activity of both BOC nanosheets and AC. This work may provide useful guidance for indoor air purification, particularly for harmful trace gases such as VOCs.

Keywords: $Bi_2O_2CO_3$; activated carbon; in situ; toluene removal; photocatalyst

Citation: Wang, X.; Chen, L.; Li, C.; Xiao, Y.; Gao, Y.; Liu, Y.; Lin, Y.; Ding, J. Enhanced Photocatalytic Performance of $Bi_2O_2CO_3$ LoadedActivated Carbon for Toluene Removal in Air. *Appl. Sci.* **2022**, *12*, 12500. https://doi.org/10.3390/app122312500

Academic Editors: Elza Bontempi, Marco Race, Avelino Núñez-Delgado, Vlasoula Bekiari, Zhien Zhang, Yaoyu Zhou and Mario Coccia

Received: 28 October 2022
Accepted: 2 December 2022
Published: 6 December 2022

1. Introduction

People usually stay indoors for the majority of the time (ca. 85~90%) during the day; thus receiving exposure to indoor air pollution from a variety of trace harmful gases such as volatile organic compounds (VOCs). Among the different VOCs, benzene, toluene, and xylene (BTX) can pose a risk of adverse health effects following long term exposure and may result in considerable harm to human health, with a high risk of developing asthma, cancers, heart disease, and lymphoma/leukemia, etc. [1–4]. Therefore, the efficient and economic disposal of BTX in the indoor environment is highly desired and has received considerable attention from researchers in recent years.

Adsorption technology is considered as a simple, economical, efficient, and environmentally friendly method for removing VOCs [5]. With adsorbents, no additional energy is needed because they are able to absorb VOCs by surface molecules at room temperature [6]. As a synthetic adsorbent, activated carbon (AC) is widely used for BTX removal due to its advantages of low costs, high adsorption capacity, high efficiency and multifunction [7–13]. Nevertheless, the process that AC removes gaseous pollutants is only a physical adsorption. If the active adsorption sites are saturated, generally AC can adsorb almost no more BTX and thus needs to be exchanged or regenerated. According to recent reports, AC can only act as a photocatalyst for the degradation of organic contaminants under UV

irradiation [14–18]. Therefore, the introduction of narrow bandgap catalytic materials is highly necessary to expand the solar absorption spectrum to the visible light region [19,20].

Among all the visible light driven photocatalysts, layered structured $Bi_2O_2CO_3$ (BOC), one of the bismuth-containing Aurivillius compounds with alternative stacking of $(Bi_2O_2)^{2+}$ thin layers separated by CO_3^{2-} groups [21–23], has been explored as a promising visible light active photocatalyst [24–26]. Furthermore, the layered structure can easily lead to the formation of 2D morphologies, such as sheet-/plate-like morphologies, which may result in excellent photocatalytic performance. In our previous work, we demonstrated the effective photocatalytic removal of toluene in air utilizing (002) oriented BOC nanosheets, which led to an almost complete degradation of toluene into CO_2 and H_2O [27,28]. These results demonstrate the promising potential of utilizing layered BOC nanostructures as photocatalyst for removing VOCs. In this work, we aim to combine the advantages of both AC and BOC as a composite catalyst for the removal of toluene in air by fabricating AC modified with BOC nanomaterials. On one hand, the AC can adsorb toluene effectively due to its large surface area. On the other hand, BOC nanostructures can function as photocatalyst for the in-situ degradation of toluene.

2. Materials and Methods

2.1. Materials

All the chemical reagents in this work were analytical-grade and used without any further purification: Bi_2O_3 (99.99%, Aladdin Industrial Corporation, Shanghai, China), HNO_3 solution (GR, Sinopharm Chemical Reagent Co., Ltd., Shanghai, China) and Na_2CO_3 (RA, Sinopharm Chemical Reagent Co., Ltd., Shanghai, China).

2.2. Synthesis of $Bi_2O_2CO_3$

In a typical experiment, 2.325 g Bi_2O_3 was dissolved in 450 mL 1 mol/L of HNO_3 solution under ultrasonication conditions. The obtained suspension was kept at 20 °C in a water bath for 1 h. Subsequently, 400 mL 0.6 mol/L Na_2CO_3 solution was added into the above suspension at a speed of 30 mL/min, until a uniform solution with pH of about 7 was reached under magnetic stirring. Then, the as-obtained powder sample was centrifuged, washed with de-ionized water and ethyl alcohol for several times, and dried at 70 °C in an oven. Finally, the powdered $Bi_2O_2CO_3$ (labeled as BOC) sample was obtained.

The synthesis process of $Bi_2O_2CO_3$ nanomaterials follows Equations (1)–(6). CO_3^{2+} is formed via a hydrolysis reaction process between Na_2CO_3 and H_2O. Bi_2O_3 is dissolved in dilute nitric acid to generate $(Bi_2O_2)^{2+}$. Then, a reaction occurs between $(Bi_2O_2)^{2+}$ and CO_3^{2+} to synthesize $Bi_2O_2CO_3$. Most of the H^+ is neutralized by CO_3^{2+} to generate CO_2 and H_2O. Only a small part of the H^+ is combined with OH^- to form H_2O. Na^+ and NO_3^- are washed off by de-ionized water.

$$HNO_3 \rightarrow H^+ + NO_3^- \quad (1)$$

$$Bi_2O_3 \xrightarrow{HNO_3} Bi_2O_2^{2+} + 2OH^- \quad (2)$$

$$Na_2CO_3 \xrightarrow{H_2O} 2Na^+ + CO_3^{2-} \quad (3)$$

$$Bi_2O_2^{2+} + CO_3^{2-} \rightarrow Bi_2O_2CO_3 \downarrow \quad (4)$$

$$2H^+ + CO_3^{2-} \rightarrow H_2O + CO_2 \quad (5)$$

$$H^+ + OH^- \rightarrow H_2O \quad (6)$$

2.3. Synthesis of BOC/AC Composites

2.325 g Bi_2O_3 was dissolved in 450 mL 1 mol/L HNO_3 solution under ultrasonication condition. The obtained suspension was kept at 20 °C in a water bath. Then, 400 mL 0.6 mol/L Na_2CO_3 solution was added into the above suspension at a speed of 30 mL/min, while stirring at a speed of 300 r/min. At the same time, different amounts (50 g, 100 g,

150 g, and 200 g) of honeycomb activated carbon (4~60 mesh, iodine value of 1050 mg/g) were added. The suspension was kept in 20 °C water bath for 6 h. Then, the product was washed with de-ionized water and ethyl alcohol several times. The as-obtained powder sample was centrifuged and dried at 70 °C in an oven. Finally, the BOC/AC composites (labeled as BOC/AC_50, BOC/AC_100, BOC/AC_150, and BOC/AC_200, respectively) were obtained.

2.4. Characterization

The X-ray diffraction (XRD) measurements were performed on a diffractometer (D8-Advance, Bruker, Karlsruhe, Germany) with monochromatized Cu Kα (λ = 1.54056 nm) radiation at a scanning speed of 0.15°/s. The microstructure of the as-obtained samples was characterized using scanning electron microscopy (SEM, JSM-7001F, JEOL, Tokyo, Japan) operated at a voltage of 5 kV. The composition of chemical elements was performed using an X-ray fluorescence (XRF, Thermo Scientific, Niton, UK).

The N_2 adsorption/desorption measurements were performed on an automated gas sorption analyzer (AutosorbiQ2, Quantachrome, Boynton Beach, FL, USA) at P/Po = 0.99 and the specific surface areas were estimated using the Brunauer–Emmet–Teller (BET) method. Before analysis, all samples were dried at 90 °C for 1 h and degassed by vacuum at 200 °C for 24 h.

2.5. Photocatalytic Activity Test

2.5.1. Photocatalytic Activity Test of $Bi_2O_2CO_3$

To prepare the sample for photocatalytic toluene removal performance in air, 0.025 g BOC was dispersed into 150 mL de-ionized water under ultrasonication for 15 min. The suspension was filtered using a 0.1 μm nylon membrane through a vacuum pump. The photocatalytic performances of the BOC samples were evaluated by toluene removal in air using a gas phase photocatalytic testing system developed by our group (China Patent, NO.202210103256.X). The reactor is a stainless steel canister and the BOC membrane was placed at the bottom of the reactor. The gas product in the reactor was analyzed at regular time intervals, using a gas chromatograph (GC), equipped with two flame-ionization detectors (FID) [28]. Toluene analysis was performed with one FID loaded with an Rt-Q-Bond Plot column (30 m × 0.25 mm, film thickness 10 μm), while CO_2 analysis was performed by the other FID loaded with a packed column (TDX-01, 3 m × 3 mm) followed by a methanizer CO_2 concentration. The gas samples were fed to the GC online through an automatic gas sampling valve.

2.5.2. Photocatalytic Activity of BOC/AC Composites

The photocatalytic performances of the BOC/AC composites were investigated using a similar system to that described in Section 2.5.1. To imitate practical applications, the stainless steel canister was replaced by a 60 L Tedlar polyvinyl fluoride (PVF) pocket in a thermostatic test chamber and kept at a constant temperature (e.g., 20 °C). Then, 3 g BOC/AC particulates was placed on the dish and into the pocket. The incident light can pass through the PVF film to the BOC/AC surface. The structure is illustrated in Figure 1.

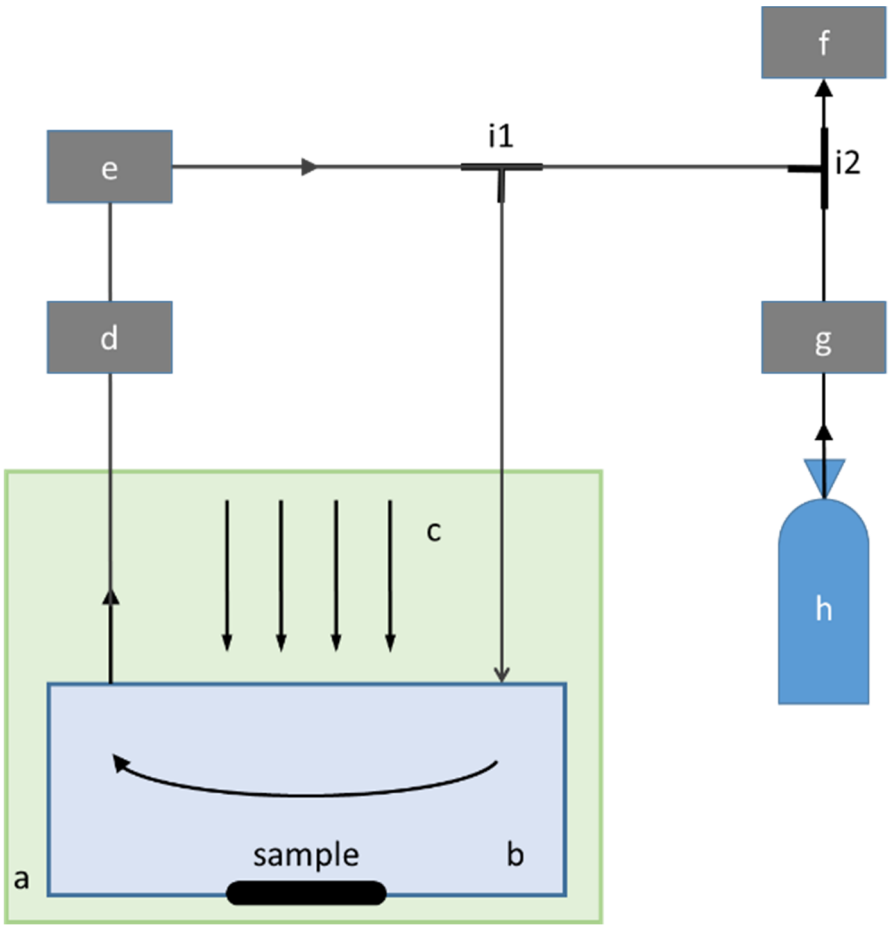

Figure 1. Schematic illustration of gas-phase photocatalysis testing system. (**a**) Thermostatic test chamber, (**b**) PVF pocket, (**c**) light source, (**d**) gas delivery pump, (**e**) gas chromatograph (GC), (**f**) vacuum pump, (**g**) gas mass flow meter, (**h**) toluene gas, and (i1–i2) three-port value.

To test the photocatalytic activity, the reaction reactor was first vacuumized by pump. Then, 60 L toluene gas (50.0 ppm in air) was injected as the target indoor pollutant. This required about 12 min. After that, the reaction reactor was kept in the dark for 0.5 h to reach the adsorption/desorption equilibrium. A 300 W xenon lamp (CEL-HXF300, Beijing China Education AuLight Technology Co., Ltd., Beijing, China) was used as the simulated sunlight source. The gas product in the reactor was analyzed at regular time intervals using GC. In addition, the toluene gas in the pocket could not flow completely to the automatic gas sampling valve of the GC at 0 min because the pipe diameter of the valve is relatively small and the gas delivery pump has just started. Thus, the toluene concentration is low. This means that the first point (at t = 0) is not 100% for all studies.

3. Results and Discussion

3.1. Characterization and Properties of $Bi_2O_2CO_3$

The crystal structure of the BOC nanomaterials prepared by chemical method was analyzed by XRD. As displayed in Figure 2, all diffraction peaks of the sample can be well indexed to the single phase of tetragonal $Bi_2O_2CO_3$ (JCPDS 41-1488) with good crystallinity, without any other impurity peaks. Moreover, the average crystal size of the BOC nanosheets was estimated to be ca. 80 nm using the XRD patterns.

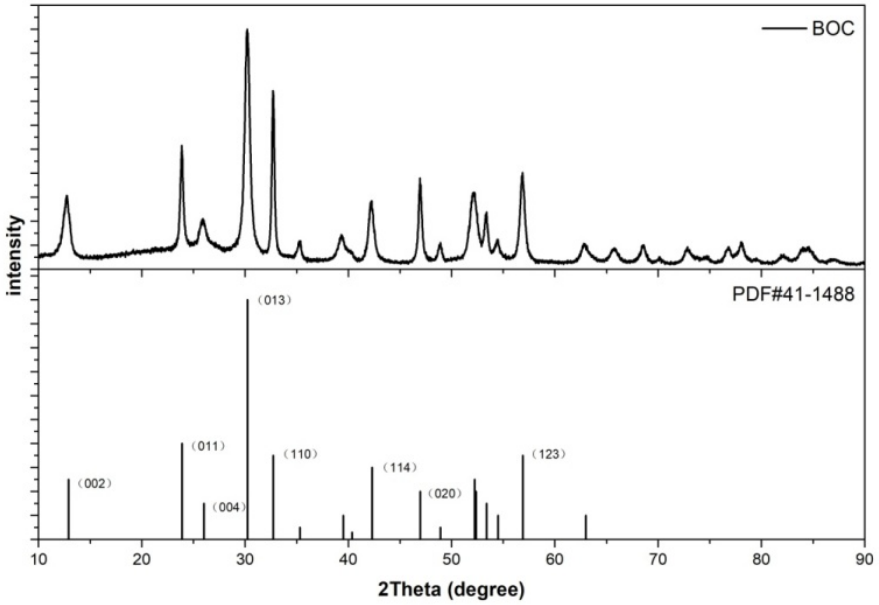

Figure 2. XRD patterns of the as-synthesized $Bi_2O_2CO_3$.

The morphology of the BOC sample was investigated by SEM. As shown in Figure 3, the BOC has a flower-like shape assembled by nanosheets during the crystallization process, with lateral sizes of several micrometers and a thickness of a few nanometers. Thus, the flower-like shape can provide more reactive sites owing to the unique layered structure of $Bi_2O_2CO_3$ [29,30].

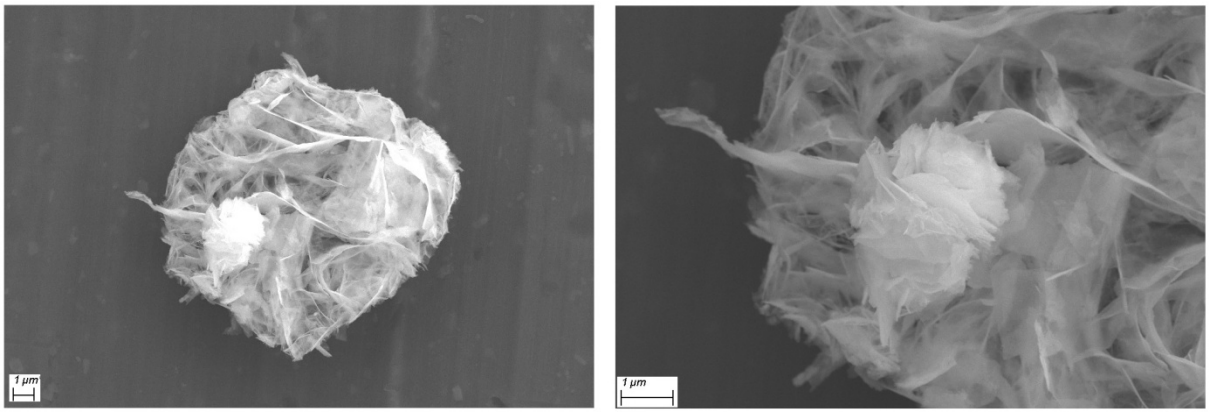

Figure 3. SEM images of $Bi_2O_2CO_3$.

The photocatalytic activity of the BOC sample for removing gaseous toluene in air was investigated at a concentration of 50.0 ppm (450 mL) under irradiation by a Xe lamp as the light source. As displayed in Figure 4, the pristine BOC sample demonstrated an excellent photocatalytic efficiency for toluene removal with a degradation rate as high as 96.8% over 3 h.

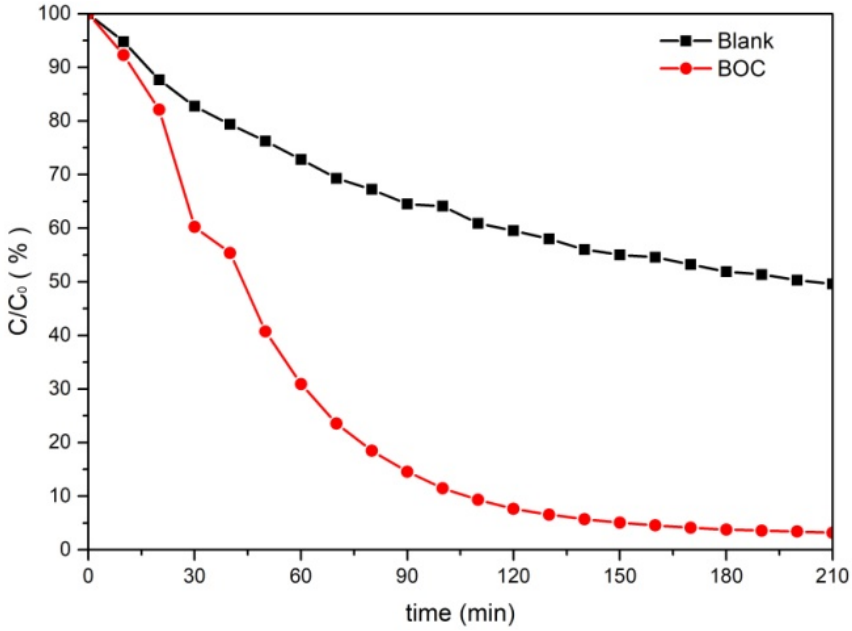

Figure 4. The photocatalytic property of $Bi_2O_2CO_3$ for toluene removal in air. The blank control experiment was performed under light illumination in the absence of catalyst.

3.2. Characterization and Propertiesof BOC/AC Composites

3.2.1. Microstructure Analysis

The microstructures of the BOC/AC and AC samples were characterized by SEM. As shown in Figure 5, the BOC/AC_50 and BOC/AC_100 samples have flower-like BOC grown on the surface of AC, with a size of ca. 5 μm (Figure 5a,b). These results demonstrate the successful growth of BOC on the surface of AC via an in-situ crystallization process. The BOC/AC_150 and BOC/AC_200 have cylinder-like morphology with a length of ca. hundreds of nanometers (Figure 5c,d). Figure 5e,f show the morphologies of the pristine AC sample, which has a porous structure with high specific surface area and good adsorption ability [31–33].

The surface area, pore volume, and pore diameter results of the as-prepared samples are shown in Figure S1 and listed in Table 1. The BOC/AC_100 sample has the highest BET surface area among all BOC/AC and AC samples, possibly because of the flower-like BOC on the surface of the AC. This is highly beneficial for promoting the photocatalytic performance by providing an abundance of active reaction sites. All samples show similar pore volume and pore diameter (1.5 nm), which is due to the use of the same matrix of AC. For these composite materials, activated carbon has excellent adsorption capability for toluene gas and $Bi_2O_2CO_3$ photocatalysis can in situ mineralize the adsorbed toluene to CO_2 and H_2O under light illumination.

3.2.2. Structure and Composition Analysis

The XRD patterns of the BOC/AC and AC are presented in Figure 6. All BOC/AC samples show similar XRD patterns (Figure 6a). In Figure 6b–d, the enlarged local XRD patterns clearly show that the peak intensity increased for BOC/AC_50 and BOC/AC_100 near $2\theta = 30.2^\circ$ and 32.7°, which are the characteristic peaks of $Bi_2O_2CO_3$ (JCPDS: 41-1488), corresponding to the (013) and (110) facets, respectively. The energy dispersive spectroscopy (EDS) elemental mapping images (Figure 7) of BOC/AC_100 sample further proves the successful growth of $Bi_2O_2CO_3$ on the surface of AC and the homogeneous elemental distribution of Bi, C, and O elements in the $Bi_2O_2CO_3$ nanosheets. To quantify the composition of different chemical elements in the composite, XRF analysis was performed, which showed that the ratio of C: O: Bi was about 94.3: 4.0: 1.7 wt.%.

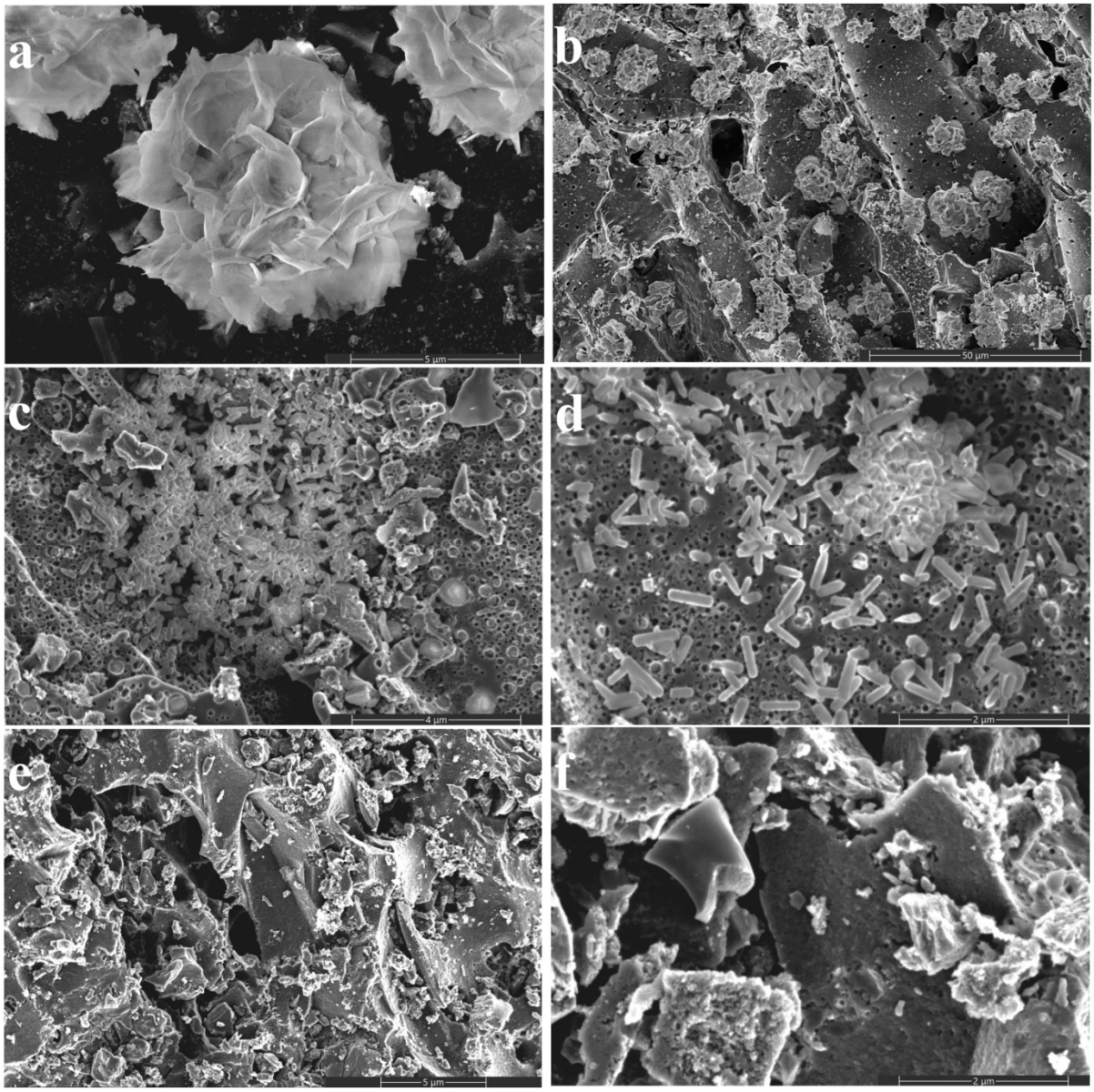

Figure 5. SEM images of BOC/AC_50 (**a**), BOC/AC_100 (**b**), BOC/AC_150 (**c**), BOC/AC_200 (**d**), and activated carbon (**e**,**f**).

Table 1. Surface area, pore volume, and pore diameter of BOC/AC.

	AC	BOC/AC_50	BOC/AC_100	BOC/AC_150	BOC/AC_200
Surface area (m^2/g)	953.8	931.8	955.3	951.2	851.4
Single point adsorption total pore volume (cm^3/g)	0.34	0.33	0.36	0.34	0.32
Average pore diameter (4V/A by BET) (nm)	1.44	1.43	1.52	1.45	1.48

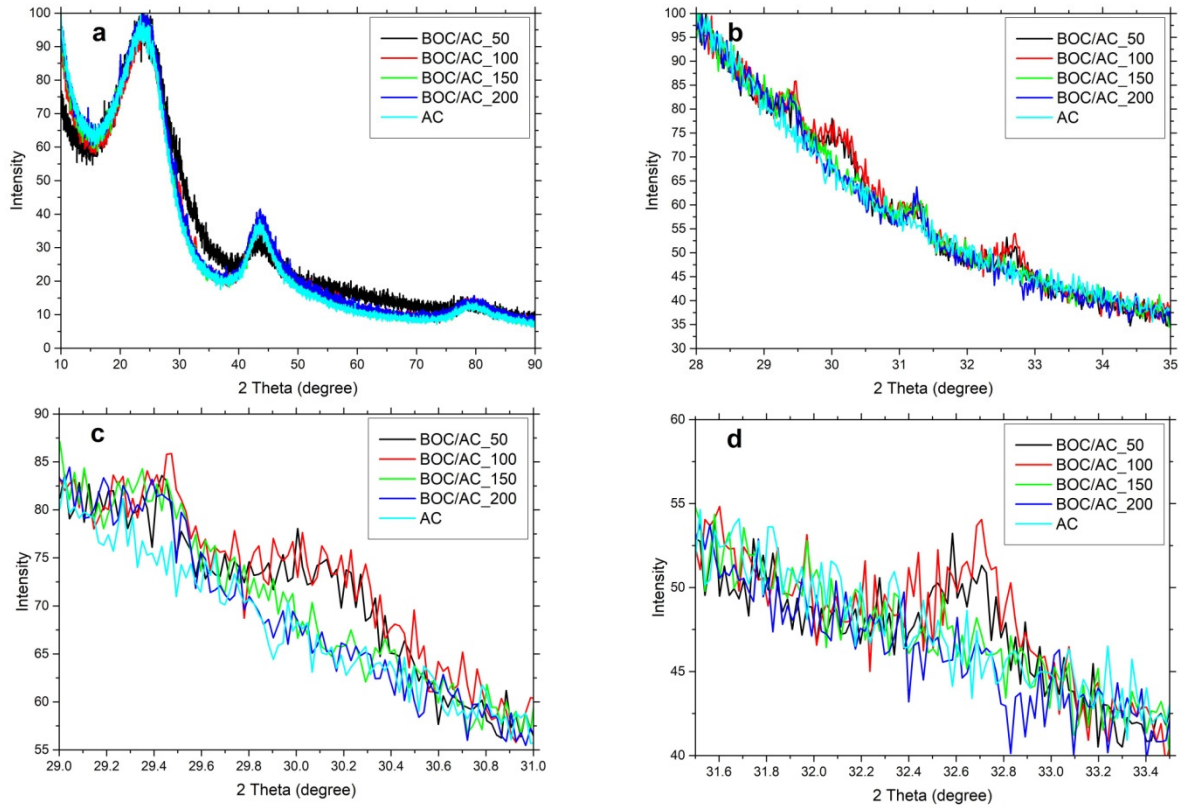

Figure 6. XRD patterns (**a**) and enlarged local XRD patterns (**b**–**d**) of the as-synthesized BOC/AC and AC.

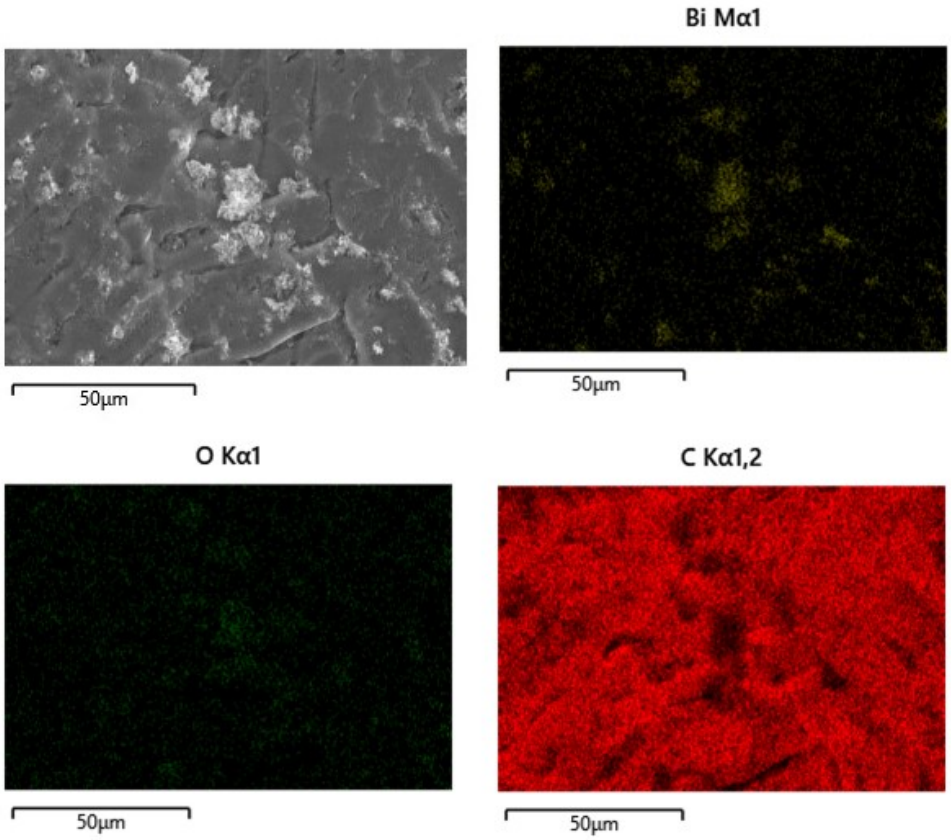

Figure 7. EDS element mapping images of BOC/AC_100.

3.2.3. Photocatalytic Properties

The photocatalytic properties of the degradation of gaseous toluene (50.0 ppm) in air over the BOC/AC composites were investigated under light illumination. As shown in Figure 8a, all samples demonstrated good removal efficiency of more than 90%. Among the BOC/AC composites, BOC/AC_100 shows the optimal efficiency with a removal rate of up to 92.2% in 3 h. The performances are comparable and higher than previously reported typical composite photocatalysts such as N-TiO_2/zeolite [34] and Fe_2O_3/In_2O_3 composite [35], showing the promising potential application of BOC/AC composite catalysts. In previous works, other methods have been used for the removal of toluene from the air, such as biofiltration [36], post-plasma catalytic technology [37], and corona discharge [38]. Compared with those methods, which are usually expensive and complex, the present BOC/AC composite has the advantages of being green and low-cost. The products of toluene degradation were detected using GC. The results demonstrate that CO_2 is the main product (Figures 8b and S2) with the highest productivity of 82.5 mg/m^3 in 3 h for BOC/AC_100, and another main product should be H_2O, on the basis that toluene is hydrocarbon. More reactive sites are provided for BOC/AC_100 due to the flower-like $Bi_2O_2CO_3$ on the surface of BOC/AC_50 and BOC/AC_100, which leads to enhanced photocatalytic performance. The photocatalytic process of the optimal sample (BOC/AC_100 composite) was investigated further. As shown in Figures 8c and S3, the toluene was completely removed in 7 h. Furthermore, the concentration of CO_2 increased significantly and reached 105.2 mg/m^3 (Figure 8d), which indicated the continuous degradation of toluene. However, the production rates of CO_2 were merely 38.3 mg/m^3 in 3 h and 55.4 mg/m^3 in 7 h for pristine AC. As we mentioned in the introduction, AC acts mainly as an adsorbent. Moreover, according to previous works, AC can also act as a photocatalyst for the degradation of organic contaminants. However, it is only active under UV irradiation with low catalytic efficiency. These results clearly show that the degradation rate of toluene is enhanced after the in-situ growth of BOC on the surface of the AC. This is attributed to the synergistic effect of the adsorption ability of AC and photocatalytic activity of both BOC and AC, demonstrating the advantage of the composite material.

The stability of BOC/AC composites (BOC/AC_100) for photocatalytic removal of toluene was evaluated by performing three experimental cycles under light illumination. As shown in Figure 8e, highly stable photocatalytic efficiency was maintained for BOC/AC_100, reaching as high as 90% for toluene removal after three cycles, which demonstrated the excellent recyclability of BOC/AC for photocatalytic toluene degradation.

In addition, we investigated the toluene removal efficiency using different amounts of BOC/AC_100 (1 g, 1.5 g, 2 g, and 3 g). As shown in Figure 8f, the photocatalytic activity was enhanced as the amount of catalyst increased, reaching the highest efficiency when 3 g of BOC/AC_100 was used.

A proposed photocatalytic reaction mechanism over the BOC/AC composites for the degradation of gaseous toluene under light irradiation can be explained as follows (Figure 9). First, the honeycomb AC matrices adsorb and capture the toluene molecules. Then, under light illumination, the electrons are excited from the valence band (VB) to the conduction band (CB) in the surface of $Bi_2O_2CO_3$ loaded Activated Carbon, leaving holes in the VB. The AC can function as electron acceptors to reduce the recombination rate of electron–hole pairs. Consequently, the excited electrons on CB in $Bi_2O_2CO_3$ can be easily transferred to the surface of AC, thus promoting the separation and migration of photo-generated charge carriers.

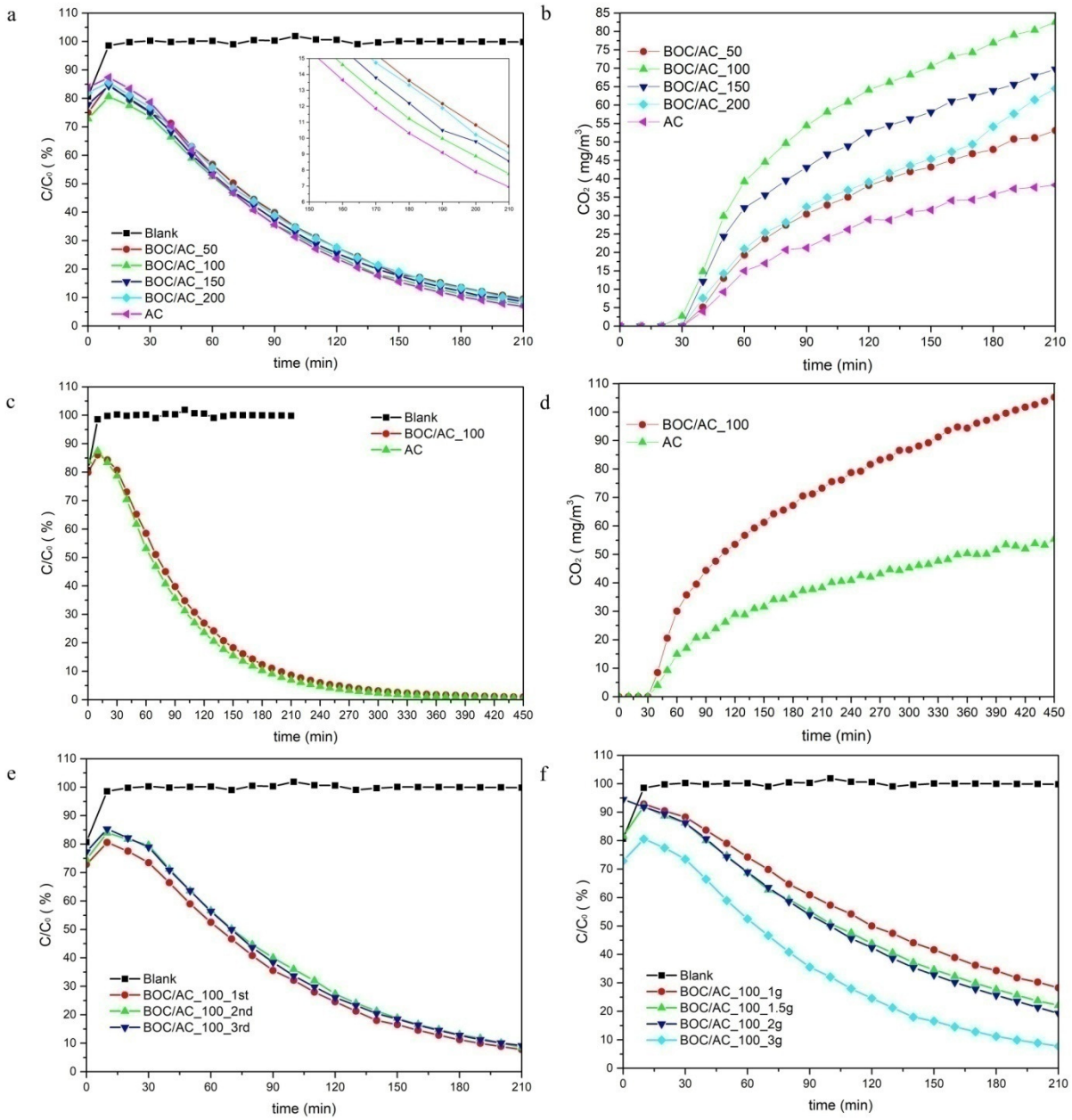

Figure 8. The photocatalytic performance of the BOC/AC samples for toluene removal in air (**a**), theCO_2 productivity of the samples (**b**), the property of BOC/AC_100 and AC for toluene removal (**c**), CO_2 productivity of BOC/AC_100 and AC (**d**), the stability of BOC/AC_100 for three cycles (**e**), and the toluene removal efficiency of the different amounts of BOC/AC_100 (**f**).

The photo-excited electrons (e^-) on the BOC and AC could reduce the O_2 adsorbed on the surface to active species of superoxide anions ($\bullet O^{2-}$). Consequently, the $\bullet O^{2-}$ active oxidizing species can oxidize toluene into intermediate products and finally into CO_2 and H_2O [39]. Meanwhile, the photo-generated holes (h^+) left on the BOC oxidize H_2O on their surface into another highly active species of hydroxyl radicals (•OH). Finally, the produced $\bullet O^{2-}$ and •OH, with strong oxidizing ability, can efficiently degrade the intermediates into CO_2 and H_2O, which are not harmful.

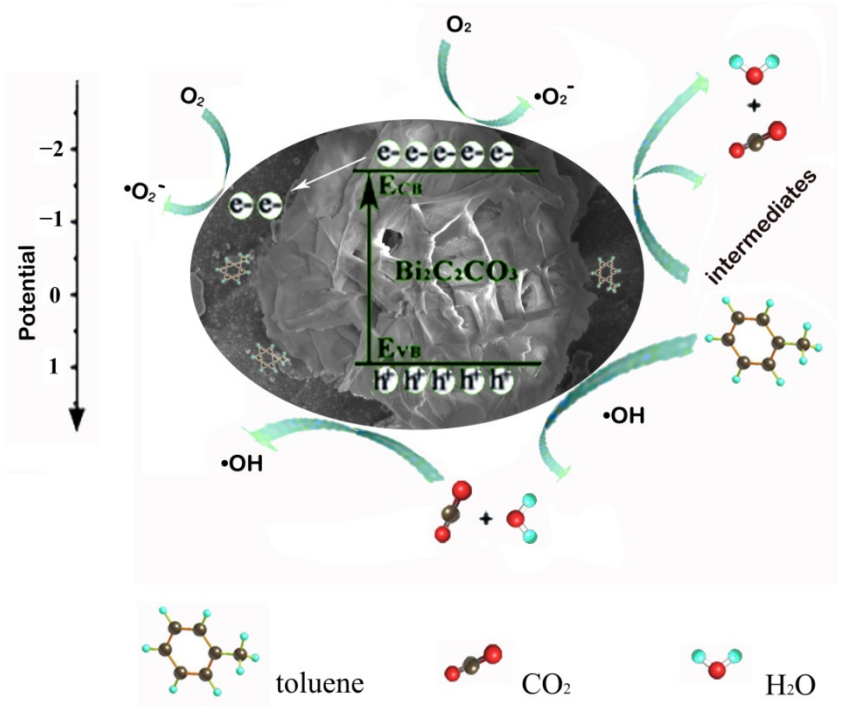

Figure 9. Photocatalytic mechanism of toluene removal using BOC/AC composite.

4. Conclusions

In summary, a novel BOC/AC nanocomposite photocatalyst was fabricated by in-situ growth of flower-shaped BOC nanosheets on the surface of activated carbon through a facile chemical method. The as-synthesized BOC/AC nanocomposite demonstrated excellent removal efficiency for toluene, with more than 90% degradation in 3 h, which is comparable and even higher than reported catalysts. Moreover, CO_2 and H_2O were confirmed as the major products. We also found that the catalytic activity was highly dependent on the loading content of BOC, with the highest performance obtained for 100 g loading. Furthermore, toluene could be completely removed after 7 h. Importantly, the photocatalytic efficiency remains constant after three cycles, demonstrating the good recyclability of the BOC/AC for photocatalytic toluene removal. The excellent photocatalytic degradation activity of the BOC/AC composite catalyst can be attributed to the synergistic effect of the adsorption ability of AC and the photocatalytic activity of both the BOC nanosheets and the AC. This work may provide useful guidance for indoor air purification, particularly for trace harmful gases such as VOCs.

Supplementary Materials: The following supporting information can be downloaded at: https://www.mdpi.com/article/10.3390/app122312500/s1, Figure S1: N2 adsorption− desorption isotherms (a) and pore size distributions (b) of AC and BOC/AC composites. Figure S2: Chromatograms of organic products at 3 h for BOC/AC_100 (a) and AC (b). Figure S3: Chromatograms of organic products at 7 h for BOC/AC_100 (a) and AC (b); Figure S4: Spectrum of the xenon lamp used.

Author Contributions: Investigation, X.W., L.C. and J.D.; Methodology, X.W., C.L., Y.G. and Y.L. (Yaochun Liu); Supervision, Y.L. (Yuanhua Lin) and J.D.; Writing and original draft, X.W. and L.C.; Review and editing, Y.L. (Yaochun Liu) and Y.X. All authors have read and agreed to the published version of the manuscript.

Funding: This research received no external funding.

Institutional Review Board Statement: Not applicable.

Informed Consent Statement: Not applicable.

Data Availability Statement: Not applicable.

Conflicts of Interest: The authors declare no conflict of interest.

References

1. Salthammer, T.; Uhde, E. (Eds.) *Organic Indoor Air Pollutants: Occurrence, Measurement, Evaluation*; WILEY-VCH: Weinheim, Germany, 2009.
2. Adan, O.C.G.; Samson, C.R. *Fundamentals of Mold Growth in Indoor Environments and Strategies for Healthy Living*; Wageningen Academic Publishers: Utrecht, The Netherlands, 2011.
3. Abadi, M.B.H.; Shirkhanloo, H.; Rakhtshah, J. Air pollution control: The evaluation of TerphApm@MWCNTs as a novel heterogeneous sorbent for benzene removal from air by solid phase gas extraction. *Arab. J. Chem.* **2020**, *13*, 1741–1751. [CrossRef]
4. Zhang, X.; Gao, B.; Fang, J.; Zou, W.; Dong, L.; Cao, C.; Zhang, J.; Li, Y.; Wang, H. Chemically activated hydrochar as an effective adsorbent for volatile organic compounds (VOCs). *Chemosphere* **2019**, *218*, 680–686. [CrossRef] [PubMed]
5. Liu, S.; Wei, W.; Wu, S.; Zhang, F.; Cheng, H. Efficient dichloromethane and toluene removal via lignin derived oxygen and nitrogen-containing activated carbons with well-developed micro-mesopore structure. *Diam. Relat. Mater.* **2022**, *124*, 108922. [CrossRef]
6. Saqlain, S.; Zhao, S.; Kim, S.Y.; Kim, Y.D. Enhanced removal efficiency of toluene over activated carbon under visible light. *J. Hazard. Mater.* **2021**, *418*, 126317. [CrossRef]
7. Kim, K.D.; Park, E.J.; Seo, H.O.; Jeong, M.G.; Kim, Y.D.; Lim, D.C. Effect of thin hydrophobic films for toluene adsorption and desorption behavior on activated carbon fiber under dry and humid conditions. *Chem. Eng. J.* **2012**, *200*, 133–139. [CrossRef]
8. Baur, G.B.; Beswick, O.; Spring, J.; Yuranov, I.; Kiwi-Minsker, L. Activated carbon fibers for efficient VOC removal from diluted streams: The role of surface functionalities. *Adsorption* **2015**, *21*, 255–264. [CrossRef]
9. Baytar, O.; Ahin, O.S.; Horoz, S.; Kutluay, S. High-performance gas-phase adsorption of benzene and toluene on activated carbon: Response surface optimization, reusability, equilibrium, kinetic, and competitive adsorption studies. *Environ. Sci. Pollut. Res.* **2020**, *27*, 26191–26210. [CrossRef] [PubMed]
10. Kutluay, S.; Baytar, O.; Ahin, O.S. Equilibrium, kinetic and thermodynamic studies for dynamic adsorption of benzene in gas phase onto activated carbon produced from Elaeagnus angustifolia seeds. *J. Environ. Chem. Eng.* **2019**, *7*, 102947. [CrossRef]
11. Zhang, G.; Lei, B.; Chen, S.; Xie, H.; Zhou, G. Activated carbon adsorbents with micro-mesoporous structure derived from waste biomass by stepwise activation for toluene removal from air. *J. Environ. Chem. Eng.* **2021**, *9*, 105387. [CrossRef]
12. Liu, X.; Zhu, H.; Gong, L.; Jiang, L.; Lin, D.; Yang, K. New insights into hierarchical pore size and level of concentration in efficient removal of toluene vapor by activated carbon. *Sci. Total Environ.* **2022**, *853*, 158719. [CrossRef]
13. Lei, B.; Liu, B.; Zhang, H.; Yan, L.; Xie, H.; Zhou, G. CuO-modified activated carbon for the improvement of toluene removal in air. *J. Environ. Sci.* **2020**, *88*, 122–132. [CrossRef] [PubMed]
14. Velasco, L.F.; Fonseca, I.M.; Parra, J.B.; Lima, J.C.; Ania, C.O. Photochemical behaviour of activated carbons under UV irradiation. *Carbon* **2012**, *50*, 249–258. [CrossRef]
15. Velo-Gala, I.; Lopez-Penalver, J.J.; Sanchez-Polo, M.; Rivera-Utrilla, J. Activated carbon as photocatalyst of reactions in aqueous phase. *Appl. Catal. B-Environ.* **2013**, *142*, 694–704. [CrossRef]
16. Velasco, L.F.; Gomis-Berenguer, A.; Lima, J.C.; Ania, C.O. Tuning the surface chemistry of nanoporous carbons for enhanced nanoconfined photochemical activity. *ChemCatchem* **2015**, *7*, 3012–3019. [CrossRef]
17. Velo-Gala, I.; L'opez-Peñalver, J.J.; S'anchez-Polo, M.; Rivera-Utrilla, J. Role of activated carbon surface chemistry in its photocatalytic activity and the generation of oxidant radicals under UV or solar radiation. *Appl. Catal. B-Environ.* **2017**, *207*, 412–423. [CrossRef]
18. Velasco, L.F.; Maurino, V.; Laurenti, E.; Fonseca, I.M.; Lima, J.C.; Ania, C.O. Photoinduced reactions occurring on activated carbons. A combined photooxidation and ESR study. *Appl. Catal. A-Gen.* **2013**, *452*, 1–8. [CrossRef]
19. Li, S.; Zhao, Z.; Li, J.; Liu, H.; Liu, M.; Zhang, Y.; Su, L.; Pérez-Jiménez, A.I.; Guo, Y.; Yang, F.; et al. Mechanically Induced Highly Efficient Hydrogen Evolution from Water over Piezoelectric SnSe nanosheets. *Small* **2022**, *18*, 2202507. [CrossRef]
20. Li, S.; Zhao, Z.; Liu, M.; Liu, X.; Huang, W.; Sun, S.; Jiang, Y.; Liu, Y.; Zhang, J.; Zhang, Z. Remarkably enhanced photocatalytic performance of Au/$AgNbO_3$heterostructures by coupling piezotronics with plasmonic effects. *Nano Energy* **2022**, *95*, 107031. [CrossRef]
21. Taylor, P.; Sunder, S.; Lopata, V.J. Structure, spectra, and stability of solid bismuth carbonates. *Can. J. Chem.* **1984**, *62*, 2863–2873. [CrossRef]
22. Chen, R.; So, M.H.; Yang, J.; Deng, F.; Che, C.-M.; Sun, H. Fabrication of bismuth subcarbonate nanotube arrays from bismuth citrate. *Chem. Commun.* **2006**, *21*, 2265–2267. [CrossRef]
23. Zhang, Q.; Yuan, S.; Xu, B.; Xu, Y.; Cao, K.; Jin, Z.; Ohno, T. A facile approach to build $Bi_2O_2CO_3$/PCNnanohybridphoto catalysts for gaseous acetaldehyde efficient removal. *Catal. Today* **2018**, *315*, 184–193. [CrossRef]
24. Madhusudan, P.; Ran, J.; Zhang, J.; Yu, J.; Liu, G. Novel urea assisted hydrothermal synthesis of hierarchical $BiVO_4$/$Bi_2O_2CO_3$ nanocomposites with enhanced visible-light photocatalytic activity. *Appl. Catal. B-Environ.* **2011**, *110*, 286–295. [CrossRef]
25. Fan, H.; Zhou, H.; Li, H.; Liu, X.; Ren, C.; Wang, F.; Li, W. Novel Ag_2CrO_4/$Bi_2O_2CO_3$ heterojunction: Simple preparation, wide visible light absorption band and excellent photocatalytic activity. *Chem. Phys.* **2019**, *517*, 60–66. [CrossRef]
26. Bai, P.; Tong, X.; Wan, J.; Gao, Y.; Xue, S. Flower-like $Bi_2O_2CO_3$-mediated selective oxidative coupling processes of amines under visible light irradiation. *J. Catal.* **2019**, *374*, 257–265. [CrossRef]

27. Ding, J.; Wang, H.; Luo, Y.; Xu, Y.; Liu, J.; Lin, Y. Oriented $Bi_2O_2CO_3$ Nanosheets with Enhanced Photocatalytic Performance for Toluene Removal in Air. *Catalysts* **2020**, *10*, 389. [CrossRef]
28. Ding, J.; Wang, H.; Luo, Y.; Xu, Y.; Liu, J.; Gao, Y.; Lin, Y. Carbon Quantum Dots Modified(002) Oriented $Bi_2O_2CO_3$ Composites with Enhanced Photocatalytic Removal of Toluene in Air. *Nanomaterials* **2020**, *10*, 1795. [CrossRef]
29. Huang, H.; Li, X.; Wang, J.; Dong, F.; Chu, P.K.; Zhang, T.; Zhang, Y. Anionic Group Self-Doping as a Promising Strategy: Band-Gap Engineering and Multi-Functional Applications of High-Performance CO_3^{2-}-Doped $Bi_2O_2CO_3$. *ACS Catal.* **2015**, *5*, 4094–4103. [CrossRef]
30. Ding, J.; Wang, H.; Xu, H.; Qiao, L.; Luo, Y.; Lin, Y.; Nan, C. Synthesis and broadband spectra photocatalytic properties of $Bi_2O_2(CO_3)_{1-x}S_x$. *Materials* **2018**, *11*, 791. [CrossRef]
31. Muthirulan, P.; Devi, C.N.; Sundaram, M.M. Synchronous role of coupled adsorption and photocatalytic degradation on CAC–TiO_2 composite generating excellent mineralization of alizarin cyanine green dye in aqueous solution. *Arab. J. Chem.* **2017**, *10*, 1477–1483. [CrossRef]
32. Alalm, M.G.; Tawfik, A.; Ookawara, S. Enhancement of photocatalytic activity ofTiO_2 by immobilization on activated carbon for degradation of pharmaceuticals. *J. Environ. Chem. Eng.* **2016**, *4*, 1929–1937. [CrossRef]
33. Elizalde-Gonz´alez, M.P.; García-Díaz, E.; Sabinas-Hern'andez, S.A. Novel preparation of carbon-TiO_2composites. *J. Hazard. Mater.* **2013**, *263*, 73–83. [CrossRef] [PubMed]
34. Wei, Z.; Sun, J.; Xie, Z.; Liang, M.; Chen, S. Removal of gaseous toluene by the combination of photocatalytic oxidation under complex light irradiation of UV and visible light and biological process. *J. Hazard. Mater.* **2010**, *177*, 814–821. [CrossRef] [PubMed]
35. Zhang, F.; Li, X.; Zhao, Q.; Zhang, Q.; Tadé, M.; Liu, S.F. Abrication of α-Fe_2O_3/In_2O_3 composite hollow microspheres: A novel hybrid photocatalyst for toluene degradation under visible light. *J. Colloid Interface Sci.* **2015**, *457*, 18–26. [CrossRef] [PubMed]
36. Darlington, A.B.; Dat, J.F.; Dixon, M.A. The Biofiltration of Indoor Air: Air Flux and Temperature Influences the Removal of Toluene, Ethylbenzene, and Xylene. *Environ. Sci. Technol.* **2001**, *35*, 240–246. [CrossRef]
37. Durme, J.V.; Dewulf, J.; Demeestere, K.; Leys, C.; Langenhove, H.V. Post-plasma catalytic technology for the removal of toluene from indoor air: Effect of humidity. *Appl. Catal. B-Environ.* **2009**, *87*, 78–83. [CrossRef]
38. Durme, J.V.; Dewulf, J.; Sysmans, W.; Leys, C.; Langenhove, H.V. A batement and degradation pathways of toluene in indoor air by positive corona discharge. *Chemosphere* **2007**, *68*, 1821–1829. [CrossRef]
39. Hennezel, O.; Pichat, P.; Ollis, D.F. Benzene and toluene gas-phase photocatalytic degradation over $H_2O$and HCL pretreated TiO_2: By-products and mechanisms. *J. Photochem. Photobiol. A-Chem.* **1998**, *118*, 197–204. [CrossRef]